Dynamic modeling of cancer cell migration in an extracellular matrix fiber network

Dynamic Modeling of Cancer Cell Migration in an Extracellular Matrix fiber network *

Min-Cheol Kim, Rohan Abeyaratne, Roger D. Kamm, and H. Harry Asada, *Member, IEEE*

***Abstract*— We have established a dynamic modeling framework for predicting spatiotemporal behaviors of cancer cell migration in the extracellular matrix (ECM). Dynamic model of cancer cell migration is integrated from four individual simulations, such as 1) filopodia penetration dynamics into the ECM, 2) intracellular mechanics including remodeling of cellular and nuclear membranes, contractile motion of actin stress fibers, and focal adhesion dynamics, 3) structural mechanics of ECM fiber networks, and 4) reaction diffusion mass transfer of degrading enzymes in the ECM. This work is motivated by experimental observations of malignant cancer cell migration, which shows that abundant filopodial formation in cancer cells is a critical characteristic of aggressive cancer cell which invade into the tissue. The dynamic model presented in this work suggests the mechanical interplay between filopodia of cancer cell and surrounding viscoelastic ECM fiber network. The work presented here compares filopodia dynamics in between soft and stiff ECMs varying its pore size.**

I. Introduction

Cancer cell migration in the stiff extracellular matrix (ECM) plays causative roles in cancer pathology since it has been known that abnormal ECM structure and changes in tissue stiffness promote cancer initiation and progress [1]. In addition, cancer cells invade and metastasize more aggressively as their surrounding ECM is stiffer [2]. In cancer cell invasion dynamics in the ECM, cancer cells migrate collectively in a similar manner of vascularizing tissues and invade surrounding tissues through the ECM. Although many tumor cells migrate collectively in tightly or loosely connected group, most malignant cancer cells migrate as individuals to metastasize into tissues [3].

In general, it has been known that there are two kinds of single cancer cell invasions including mesenchymal and amoeboid cancer cell migrations. Depending on surrounding ECM's mechanical properties, such as its pore sizes, they adjust their morphologies. For example, when ECM fibers are tightly crosslinked with small pore sizes, mesenchymal cancer cells secrete matrix metalloproteinase (MMP) family to degrade local ECM in which cellular membrane interact with. In contrast, cancer cells can deform their morphologies like amoeboid when pore sizes of surrounding ECM are large, then they squeeze into ECM fiber network [4].

Dynamics of mesenchymal cancer invasion are significantly different from that of amoeboid cancer invasion in the aspect of abundant filopodial formations at the leading edge of mesenchymal cancer cell. Filopodia are finger-like actin-rich plasma membrane protrusions that are linked to enhancement of directed cell migration [5]. In addition, filopodia play two critical roles in interacting with the ECM as sensors they probe the environment, and as mechanical actuators they bind to ECM fibers and generate strong traction forces by a feedback control of contractile actin-myosin machineries in filopodia. However, distinct differences of filopodia penetration dynamics in between both soft and stiff ECMs remains poorly understood.

To address this question, we first construct a computational model of single cancer cell invasion into a viscoelastic ECM fiber network that predicts the interplay between filopodial traction generation and the remodeling of viscoelastic substrate. We integrated the following four key components: 1) filopodia penetration dynamics, 2) intracellular dynamics [6][7], including focal adhesion dynamics, actin motor activity of stress fibers (SFs), and cellular and nuclear membrane mechanics 3) ECM fiber dynamics [8], and 4) reaction diffusion mass transfer models of MMP family in the domain of ECM to degrade crosslinked ECM fibers. To our knowledge, this is the first report of integrated cancer cell migration model that takes into account various motions of filopodia phases interacting with a ECM fiber network.

II. Dynamical Model

A. Dynamics of single cancer cell migration

We construct four different modules of simulations (**Figure 1A**), including filopodia penetration dynamics in 3D ECM, intracellular dynamics [6][7], intercellular dynamics, viscoelastic ECM fiber dynamics [8], and reaction diffusion mass transfer phenomena to elucidate the mesenchymal cancer cell migration behaviors in the viscoelastic ECM during cancer metastasis process. Dynamic models of these three modules are constructed using the Lagrange approach, and a module of reaction diffusion mass transfer is constructed using a finite volume method (FVM) [9].

We model the geometric structure of a cell as a triple meshes structure: the outer, middle, and inner meshes

* Manuscript received September 19, 2016. This material is based on work supported in part by the EBICS Science and Technology Center. The work is also supported by the Singapore-MIT Alliance for Research and Technology, Bio-Systems and Micromechanics IRG.

Min-Cheol Kim is with the Departments of Mechanical Engineering, Massachusetts Institute of Technology, Cambridge, MA 02139 USA (phone: 617-253-3772; e-mail: mincheol@mit.edu).

Rohan Abeyaratne is with the Departments of Mechanical Engineering, Massachusetts Institute of Technology, Cambridge, MA 02139 USA (phone: 617.253.0066; e-mail: rohan@mit.edu)..

Roger D. Kamm is with the Departments of Mechanical Engineering and Biological Engineering, Massachusetts Institute of Technology, Cambridge, MA 02139 USA (phone: 617.253.5330; e-mail: rdkamm@mit.edu).

H. Harry Asada is with the Departments of Mechanical Engineering, Massachusetts Institute of Technology, Cambridge, MA 02139 USA (phone: 617-253-6257; e-mail: asada@mit.edu).

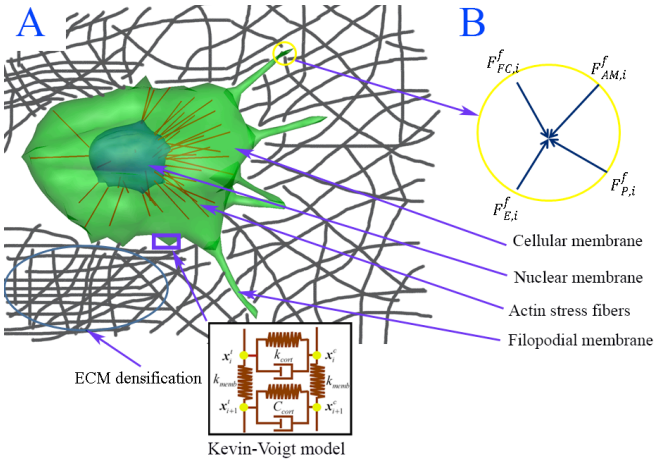

Figure 1: Dynamic model of cancer cell migration in an elastic ECM fiber network. A) Integrated cancer cell migration model consisting of cellular membrane, nuclear membrane, actin stress fibers, and filopodial membrane. The cellular membrane is not only connected by actin stress fibers (SFs), but also anchored to the elastic substrate by forming focal adhesions (FAs), and viscoelastic behaviors in cellular membrane is modeled using Kelvin-Voigt model. B) The free body diagram of the *i-th* filopodial node in the circle marked in A) where four external forces are acting.

represent the cellular , transduce, and nuclear membranes, respectively. Each mesh consists of 546 nodes connected elastically to adjacent nodes. Viscoelastic behaviors in the cellular membrane is modeled using the Kevin-Voigt model (a spring and a dashpot in **Figure 1A**), that is, the cellular membrane and the transduce layer are coupled with the actin cortex at the *i*-th node. The middle and outer mesh nodes may be connected when SFs are formed between the nucleus and the transduce layers. Multiple transmembrane integrin molecules (100 integrins per a node) are clustered together and placed at each node on the outer mesh of cellular and filopodial membranes. They can bind to ECM fibers, forming focal adhesions on the cellular membrane, to which actin stress fibers (SF) are connected, or forming focal complexes on the filopodial membrane. An example of focal complexes is shown in **Figure 1B**.

B. Filopodia penetration dynamics

We assume that filopodia penetration dynamics into 3D ECM consists of four different phases, such as 1) an outgrowing phase due to protrusive actin polymerization, 2) a retractile phase due to zero or weak focal complex (FC) force at the filopodial tip, 3) a contractile phase due to strong FC forces at the filopodial tip, and 4) a tugging phase due to the attachment of a filopodial tip to an nearby ECM. Depending on the strength and spatiotemporal properties of the FC formation, the bond of FC at the filopodial tip either ruptures or results in the generation of a significant traction force. This phase plays a critical role in switching among the other phases and coordination of the diverse filopodial dynamics, leading to either success or failure of cell migration depending on local ECM conditions. To solve the filopodia penetration dyanamics into 3D ECM, a dynamic equation at the *i*-th node on the filopodial membrane can be expressed as

$$C_f \frac{d\boldsymbol{x}_i^f}{dt} = \boldsymbol{F}_{E,i}^f + \boldsymbol{F}_{FC,i}^f + \boldsymbol{F}_{P,i}^f + \boldsymbol{F}_{AM,i}^f, \quad i = 1, \cdots, N_f. \quad (1)$$

where C_f is a coefficient of dissipation energy for the filopodial membrane (0.001 N s m^{-1}), $\boldsymbol{F}_{E,i}^f$, $\boldsymbol{F}_{FC,i}^f$, $\boldsymbol{F}_{P,i}^f$, and $\boldsymbol{F}_{AM,i}^f$ are an elastic force, a focal complex force, an actin polymerization force, and an actin-myosin contractile force at the *i*-th node of the filopodial membrane, respectively. N_f is total number of nodes on the filopodial membrane. $\boldsymbol{F}_{E,i}^f$ is derived from total elastic energy of filopodial membrane. Two types of elastic energies are considered here. One is the elastic energy associated with line element changes between nodes, and the other is the elastic energy associated with area element changes between triangular nodes. These two elastic energies are expressed as:

$$E_L^f = \frac{\kappa_L^f}{2} \sum_{j=1}^{line} \left(L_j^f - L_j^{f,0} \right)^2, \quad (2a)$$

$$E_A^f = \frac{\kappa_A^f}{2} \sum_{j=1}^{element} \left(\frac{A_j^f - A_j^{f0}}{A_j^{f0}} \right)^2 A_j^{f0}, \quad (2b)$$

where E_L^f and E_A^f are total elastic energies associated with line and area elements in the filopodial membrane, respectively. κ_L^f and κ_A^f are stiffness of line (5.0×10^{-5} N/m) and area (1.0×10^{-4} N/m^2) elements in the filopodia, respectively. L_j^f and A_j^f are the length and area at the stressed state, and L_j^{f0} and A_j^{f0} are the length and area at the unstressed state, respectively. Elastic force $\boldsymbol{F}_{E,i}^f$ at the *i*-th node on the filopodial membrane can be obtained by differentiating two total energies (virtual energy method) as following:

$$\begin{aligned} \boldsymbol{F}_{E,i}^f &= -\frac{\partial E_L^f}{\partial \boldsymbol{x}_i^f} - \frac{\partial E_A^f}{\partial \boldsymbol{x}_i^f} \\ &= -\kappa_L^f \sum_{j=1}^{line} \left(L_j^f - L_j^{f,0} \right) \frac{\partial L_j^f}{\partial \boldsymbol{x}_i^f} - \kappa_A^f \sum_{j=1}^{element} \left(\frac{A_j^f - A_j^{f0}}{A_j^{f0}} \right) \frac{\partial A_j^f}{\partial \boldsymbol{x}_i^f}. \end{aligned} \quad (3)$$

Focal complex force $\boldsymbol{F}_{FC,i}^f$ at the *i*-th node on the filopodial membrane can be expressed as

$$\boldsymbol{F}_{FC,i}^f = n_{b,i} \kappa_{LR} \left(L_b - \lambda \right) \hat{\boldsymbol{n}}_{R,i}^f \quad (4)$$

where $n_{b,i}$ is the number of integrin-collagen bonds, κ_{LR} is the spring constant of a single ligand-receptor bond (~1 pN/nm), L_b is the average stretched length of the ligand-receptor bonds, λ is an unstressed length of bonds (~30nm) and $\hat{\boldsymbol{n}}_{R,i}^f$ is a unit vector at the local surface of the *i*-th filopodial (**Figure 2**). Here $\left(L_b - \lambda \right)$ represents the stretched distance from the equilibrium. $n_{b,i}$ is calculated by Bell's equation [10].

The actin polymerization force, $\boldsymbol{F}_{P,i}^f$, is only nonzero during the outgrowing phase. The polymerization of actin filopodia in a filopodium generate protrusive force against the membrane of the filopodial tip, and the magnitude of $\boldsymbol{F}_{P,i}^f$ is assumed to be ~2 nN since the diameter of filopodium is ~ 300nm consisting of > 30 actin filaments. The direction of $\boldsymbol{F}_{P,i}^f$ is

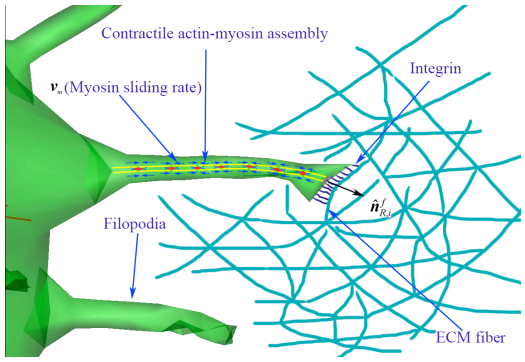

Figure 2: Mechanical interplay between filopodia and ECM fiber. Schematic showing integrin molecules on the filopodial membrane interacting with an extracellular matrix fiber, and illustrating a stochastic ligand-receptor bonding process at the focal complex site. Also, this schematic shows that filopodia can sense the strength of external force (or the magnitude of $\boldsymbol{F}^f_{FC,i}$) from the surrounding ECM fibers, and adjust their myosin sliding rates ($\boldsymbol{v}_m$) with a function of the strength of external force. Contractile actin-myosin assemblies are located along to the shaft of filopodia. Small blue arrows on the actin-myosin assemblies indicate directions of contractile actin filaments, small blue lines are integrin molecules at the tip of filopodium.

assumed to be identical to the direction of normal unit vector at the filopodial root.

The filopodial model is geometrically composed of N_{AM} compartments of actin-myosin (AM) assemblies; the first compartment is attached to the root of filopodium and the last compartment is connected to the tip of filopodium (**Figure 2**). We model filopodial contractile motion using AM assemblies as shown in **Figure 2**. We assume that the stiffness of an AM is variable as the length of the AM ($L^1_{AM,j}$) is decreased by time. Thus, the length of each AM contracts at both ends according to the myosin II sliding rate, and rate of change for $L^1_{AM,j}$ is expressed as, $\dfrac{dL^1_{AM,j}}{dt} = -2v_{m,j}$. The stiffness of an AM is expressed as, $\kappa_{AM,j} = \dfrac{E_{AM}A_{AM}}{L^1_{AM,j}}$, $j = 1..N_{AM}$. Note that $L^1_{AM,j}$ is an unstressed length of a single compartment of the j-th AM. In addition, to incorporate mechanical interplay between the filopodia and ECM, we adopt the force-velocity relation of muscle myosin II as following:

$$v_m = v_{m0}\frac{F_{stall} - F_{TR}}{F_{stall} + c_m F_{TR}} \tag{5}$$

where v_{m0} is the sliding rate of myosin in the absence of load, F_{stall} is the stall force of 1 nN, c_m is a dimensionless myosin parameter of 0.1, and F_{TR} is the magnitude of sensed elastic force from the ECM at the tip of filopodium. The total elastic energy stored in the AMs in the filopodium is given by

$$\mathrm{H}_{AM} = \sum_{j=1}^{N_{AM}}\left[\frac{\kappa_{AM,j}}{2}\left(d_{AM,j} - L^1_{AM,j}\right)^2\right] \tag{6}$$

where $d_{AM,j}$ represents the distance of the j-th contractile AM compartment under tension. Using the virtual work theory, forces due to contractile myosin motor activity at the j-th node of filopodial shaft is given by

$$\begin{aligned}\boldsymbol{F}^f_{AM,j} &= -\frac{\partial \mathrm{H}_{AM}}{\partial \boldsymbol{x}^f_j} = -\kappa_{AM,j}\left(d_{AM,j} - L^1_{AM,j}\right)\frac{\partial d_{AM,j}}{\partial \boldsymbol{x}^f_j} \\ &+\kappa_{AM,j+1}\left(d_{AM,j+1} - L^1_{AM,j+1}\right)\frac{\partial d_{AM,j+1}}{\partial \boldsymbol{x}^f_{j+1}}.\end{aligned} \tag{7}$$

C. *Intracellular dynamics*

The intracellular dynamics is another key mechanisms involved in cancer cell migration in 3D ECM. The essential equations in the model include: 1) an equation for stochastic focal adhesion (FA) dynamics based on Monte-Carlo simulations of ligand-receptor bonds, 2) three equations for deformations of double viscoelastic cellular membranes: an outer cell membrane and an inner transduce membrane, and a nuclear membrane, 3) an equation describing the contractile motion of actin stress fibers, which is extended from FAs on the cortical surface to the nuclear membrane, and 4) lamellipodium protrusion by actin polymerization. Among them, the major extension in the model of intracellular mechanics presented here is FAs dynamics in 3-D ECM fiber network model. The FA force acts between the i-th integrin node on the cellular membrane and points of ECM fibers where the extension of the unit vector normal to the cellular membrane interacts with the nearest point of ECM fibers. A dynamic equation at the i-th node on the outer cellular membrane can be expressed as

$$\begin{aligned}&\left(C_c + C_{cort}\right)\frac{d\boldsymbol{x}^c_i}{dt} - C_{cort}\frac{d\boldsymbol{x}^t_i}{dt} \\ &= \boldsymbol{F}^c_{FA,i} + \boldsymbol{F}^c_{E,i} + \boldsymbol{F}^c_{L,i} + \boldsymbol{F}^c_{T,i}, \quad i = 1,\cdots,N_c\end{aligned} \tag{8}$$

where C_c and C_{cort} are coefficients of dissipation energy for the outer cell membrane (0.001 N s m^{-1}) and the actin cortex (0.001 N s m^{-1}), respectively. In addition, C_{cort} is a drag coefficient associated with viscoelastic behaviors in the actin cortex (0.001 N s m^{-1}). $\boldsymbol{F}^c_{FA,i}$, $\boldsymbol{F}^c_{E,i}$, $\boldsymbol{F}^c_{L,i}$, and $\boldsymbol{F}^c_{T,i}$ are a FA force, an elastic force, a lamellipodium force, and a transduce force representing the elastic force of actin cortex at the i-th node of the outer cell membrane, respectively. The FA force, $\boldsymbol{F}^c_{FA,i}$, can be expressed in a similar manner of focal complex force at the filopodia (See Eq. (4)):

$$\boldsymbol{F}^c_{FA,i} = n_{b,i}\kappa_{LR}\left(L_b - \lambda\right)\hat{\boldsymbol{n}}^c_{R,i}. \tag{9}$$

The elastic force, $\boldsymbol{F}^c_{E,i}$, is also can be similarly expressed like Eq. (3):

$$\boldsymbol{F}^c_{E,i} = -\kappa^c_L\sum_{j=1}^{line}\left(L^c_j - L^{c,0}_j\right)\frac{\partial L^c_j}{\partial \boldsymbol{x}^c_i} - \kappa^c_A\sum_{j=1}^{element}\left(\frac{A^c_j - A^{c0}_j}{A^{c0}_j}\right)\frac{\partial A^c_j}{\partial \boldsymbol{x}^c_i}. \tag{10}$$

Normally, cells experience a small protrusive pressure that results from osmotic pressure or actin branches stimulated by activated arp2/3. Here we assume that the magnitude of the lamellipodium force, $\boldsymbol{F}^c_{L,i}$, at the i-th cytoskeleton node is constant at 300 pN, and exists at only leading edges of the cell.

The transduce force, $\boldsymbol{F}_{T,i}^{c,k}$ is an elastic force in the Kevin-Voigt model and expressed as

$$\boldsymbol{F}_{T,i}^{c} = -k_{cort}\left(L_{T,i}^{1} - L_{T,i}^{0}\right)\frac{\partial L_{T,i}^{1}}{\partial \boldsymbol{x}_{i}^{c}} \tag{11}$$

where k_{cort} is an effective spring constant of line element of the actin cortex (8.0×10^{-3} N/m), $L_{T,i}^{k,1}$ is the length of the *i*-th line in the actin cortex, and it is updated at every time-step. $L_{T,i}^{k,0}$ is its relaxed (zero force) length (500 nm).

A dynamic equation at the *i*-th node of the inner transduce membrane can be expressed as

$$\begin{aligned} &-C_{cort}\frac{d\boldsymbol{x}_{i}^{c}}{dt} + \left(C_{t} + C_{cort}\right)\frac{d\boldsymbol{x}_{i}^{t}}{dt} \\ &= \boldsymbol{F}_{E,i}^{t} + \boldsymbol{F}_{SF,i}^{t} + \boldsymbol{F}_{T,i}^{t}, \quad i = 1,\cdots,N_{t} \end{aligned} \tag{12}$$

where C_t is a coefficient of dissipation energy for the inner transduce membrane (0.001 N s m^{-1}), and N_t is the number of the inner transduce membrane. $\boldsymbol{F}_{E,i}^{t}, \boldsymbol{F}_{SF,i}^{t}$, and $\boldsymbol{F}_{T,i}^{t}$ are an elastic force, actin stress fiber (SF) force, and a transduce force at the *i*-th node of the inner transduce membrane respectively. The elastic force, $\boldsymbol{F}_{E,i}^{t}$, can be expressed in a similar manner of $\boldsymbol{F}_{E,i}^{c}$ as

$$\boldsymbol{F}_{E,i}^{t} = -\kappa_{L}^{t}\sum_{j=1}^{line}\left(L_{j}^{t} - L_{j}^{t,0}\right)\frac{\partial L_{j}^{t}}{\partial \boldsymbol{x}_{i}^{t}} - \kappa_{A}^{t}\sum_{j=1}^{element}\left(\frac{A_{j}^{t} - A_{j}^{t0}}{A_{j}^{t0}}\right)\frac{\partial A_{j}^{t}}{\partial \boldsymbol{x}_{i}^{t}}. \tag{13}$$

The actin SF force, $\boldsymbol{F}_{SF,i}^{t}$, can be similarly expressed like the Eq. (7):

$$\begin{aligned} \boldsymbol{F}_{SF,j}^{t} &= -\frac{\partial \mathrm{H}_{SF}}{\partial \boldsymbol{x}_{j}^{t}} = -\kappa_{SF,j}\left(d_{SF,j} - L_{SF,j}^{1}\right)\frac{\partial d_{SF,j}}{\partial \boldsymbol{x}_{j}^{t}} \\ &+\kappa_{SF,j+1}\left(d_{SF,j+1} - L_{SF,j+1}^{1}\right)\frac{\partial d_{SF,j+1}}{\partial \boldsymbol{x}_{j+1}^{t}}. \end{aligned} \tag{14}$$

The transduce force, $\boldsymbol{F}_{T,i}^{t}$, is expressed as

$$\boldsymbol{F}_{T,i}^{t} = -\boldsymbol{F}_{T,i}^{c}. \tag{15}$$

Lastly, a dynamic equation at the *i*-th node of the nuclear membrane can be expressed as

$$C_{n}\frac{d\boldsymbol{x}_{i}^{n}}{dt} = \boldsymbol{F}_{E,i}^{n} + \boldsymbol{F}_{SF,i}^{n}, \quad i = 1,\cdots,N_{n} \tag{16}$$

where C_n is a coefficient of dissipation energy for the nuclear membrane (0.001 N s m^{-1}), and N_n is the number of nodes in the nuclear membrane. $\boldsymbol{F}_{E,i}^{n}$ and $\boldsymbol{F}_{SF,i}^{n}$ are an elastic force and a SF force at the *i*-th node of the nuclear membrane. The elastic force, $\boldsymbol{F}_{E,i}^{n}$, can be expressed in a similar manner of the Eq (10) as

$$\boldsymbol{F}_{E,i}^{n} = -\kappa_{L}^{n}\sum_{j=1}^{line}\left(L_{j}^{n} - L_{j}^{n,0}\right)\frac{\partial L_{j}^{n}}{\partial \boldsymbol{x}_{i}^{n}} - \kappa_{A}^{n}\sum_{j=1}^{element}\left(\frac{A_{j}^{n} - A_{j}^{n0}}{A_{j}^{n0}}\right)\frac{\partial A_{j}^{n}}{\partial \boldsymbol{x}_{i}^{n}}. \tag{17}$$

The details of parameters in the above equation can be found in the literature [6]. The actin SF force, $\boldsymbol{F}_{SF,i}^{n}$, can be expressed as

$$\boldsymbol{F}_{SF,i}^{n} = -\boldsymbol{F}_{SF,k}^{t}. \tag{18}$$

In particular, Equations (8) and (12) can be coupled with the viscoelastic actin cortex using kelvin-voigt model (**Figure 1**). To solve these ordinary differential equations numerically, they should be converted with respect to vectors $\left\{\frac{d\boldsymbol{x}_{i}^{c}}{dt}, \frac{d\boldsymbol{x}_{i}^{t}}{dt}\right\}^{T}$ as followings:

$$\begin{pmatrix} \frac{d\boldsymbol{x}_{i}^{c}}{dt} \\ \frac{d\boldsymbol{x}_{i}^{t}}{dt} \end{pmatrix} = [C]^{-1}\begin{pmatrix} \boldsymbol{F}_{FA,i}^{c} + \boldsymbol{F}_{E,i}^{c} + \boldsymbol{F}_{L,i}^{c} + \boldsymbol{F}_{T,i}^{c} \\ \boldsymbol{F}_{E,i}^{t} + \boldsymbol{F}_{SF,i}^{t} + \boldsymbol{F}_{T,i}^{t} \end{pmatrix} \quad i = 1,\cdots,N_{c}. \tag{19}$$

where $[C]^{-1} = \frac{1}{C_{c}C_{t} + C_{cort}(C_{c} + C_{t})}\begin{pmatrix} C_{t} + C_{cort} & C_{cort} \\ C_{cort} & C_{c} + C_{cort} \end{pmatrix}$.

D. Dynamics of ECM fibers

We assume the ECM fiber network to be composed of elastic ECM fibers and crosslinks, which make strong bonds between adjacent fibers. The elastic energy stored in the ECM fiber network can be expressed in terms of the stretching and bending properties of the constituent fibers. In addition, cells and filopodia interact with ECM fiber network by forming focal adhesion and focal complex, respectively. Thus, forces exerted on the *i*-th node in a single ECM fiber are elastic force $\boldsymbol{F}_{E,i}^{e}$, focal adhesion force $\boldsymbol{F}_{FA,i}^{e}$ (cell membrane), and focal complex force $\boldsymbol{F}_{FC,i}^{e}$ (filopodial membrane). A dynamic equation at the *i*-th ECM fiber node can be expressed as

$$C_{e}\frac{d\boldsymbol{x}_{i}^{e}}{dt} = \boldsymbol{F}_{FA,i}^{e} + \boldsymbol{F}_{FC,i}^{e} + \boldsymbol{F}_{E,i}^{e}, \quad i = 1,\cdots,N_{e}. \tag{20}$$

where N_e is the total number of nodes in ECM fiber network. The stretching modulus of a fiber is given by $\kappa_{f,s}^{e}\left(= E_{f}^{e}A_{f}\right)$, where E_f^e and $A_f\left(=\pi r_{f}^{2}\right)$ are the Young's modulus (1 MPa) and the cross-sectional area of a single fiber, respectively. The bending modulus of a fiber is given by $\kappa_{f,b}^{e}\left(= E_{f}I_{f}\right)$, where $I_f\left(=\pi r_{f}^{4}/4\right)$[11]. The stretching elastic energy of the *j*-th node in fiber network is given as a function of the difference between the stressed (L_{ij}^{e}) and unstressed (L_{j}^{e0}) lengths, and the bending elastic energy as the one of stressed (θ_{j}^{e}) and unstressed (θ_{j}^{e0}) angles at the *j*-th node between two segments in a fiber. The total elastic energy in the ECM fiber network can be expressed as following:

$$\mathrm{H}_{f}^{e} = \frac{\kappa_{f,s}^{e}}{2}\sum_{j=1}^{N_{f}^{e}}\frac{\left(L_{j}^{e} - L_{j}^{e0}\right)^{2}}{L_{j}^{e0}} + \frac{\kappa_{f,b}^{e}}{2}\sum_{j=1}^{N_{f}^{e}}\frac{\left(\theta_{j}^{e} - \theta_{j}^{e0}\right)^{2}}{L_{j}^{e0}}. \tag{21}$$

Similarly, the elastic force at the *j*-th node in the fiber network can be derived by using the virtual work theory:

$$\boldsymbol{F}_{E,i}^{e} = -\frac{\partial \mathrm{H}_{f}^{e}}{\partial \boldsymbol{x}_{i}^{e}} = -\boldsymbol{\kappa}_{f,s}^{e}\sum_{k=1}^{N_e}\frac{\left(L_k^e - L_k^{e0}\right)}{L_k^{e0}}\frac{\partial L_k^e}{\partial \boldsymbol{x}_i^e} - \boldsymbol{\kappa}_{f,b}^{e}\sum_{k=1}^{N_e}\frac{(\theta_k^e - \theta_k^{e0})}{L_k^{e0}}\frac{\partial \theta_k^e}{\partial \boldsymbol{x}_i^e} \quad (21)$$

In addition, $\boldsymbol{F}_{FA,i}^{e}$ and $\boldsymbol{F}_{FC,i}^{e}$ are coupled with intracellular mechanics and filopodia penetration dynamics through two equations of $\boldsymbol{F}_{FA,i}^{e} + \boldsymbol{F}_{FA,k}^{c} = 0$, and $\boldsymbol{F}_{FC,i}^{e} + \boldsymbol{F}_{FC,m}^{f} = 0$, respectively.

E. Reaction-diffusion mass transfer in ECM

To consider chemical interactions of the ECM fiber network with a cancer cell, we model the degradation, proteolysis, and haptotaxis of the ECM fiber network. Six reaction-diffusion equations for concentrations of MMP-2 (ϕ_1), TIMP-2 (ϕ_2), MT1-MMP (ϕ_3), a ternary complex of MT1-MMP: TIMP-2:proMMP-2 (ϕ_4) (12), ligands (ϕ_5) (or collagen molecules) and ECM (ϕ_6) are numerically solved using Finite Volume Method (FVM). Constitutive partial differential equations for the six biochemical concentrations are summarised in followings [12]:

$$\frac{\partial \phi_1}{\partial t} = \nabla\cdot\left(D_{\phi_1}\nabla\phi_1\right) - k_{\phi_1:\phi_2}^{on}\phi_1\phi_2 + k_{\phi_3:\phi_4}^{on}\phi_3\phi_4 - k_{\phi_1}^{decay}\phi_1 - k_{\phi_6}^{deg}\phi_1\phi_6 \quad (22)$$

$$\frac{\partial \phi_2}{\partial t} = \nabla\cdot\left(D_{\phi_2}\nabla\phi_2\right) - k_{\phi_1:\phi_2}^{on}\phi_1\phi_2 - k_{\phi_2:\phi_3}^{on}\phi_2\phi_3 + k_{\phi_4}^{off}\phi_4 + \alpha_{\phi_2}\left(x_{base}^{f}\right)\phi_5 \quad (23)$$

$$\frac{\partial \phi_3}{\partial t} = -k_{\phi_2:\phi_3}^{on}\phi_2\phi_3 + k_{\phi_4}^{off}\phi_4 - k_{\phi_3}^{decay}\phi_3 + \alpha_{\phi_3}\left(x_{base}^{f}\right)\phi_5 \quad (24)$$

$$\frac{\partial \phi_4}{\partial t} = k_{\phi_2:\phi_3}^{on}\phi_2\phi_3 + k_{\phi_3:\phi_4}^{on}\phi_3\phi_4 - k_{\phi_4}^{off}\phi_4 \quad (25)$$

$$\frac{\partial \phi_5}{\partial t} = \nabla\cdot\left(D_{\phi_5}\nabla\phi_5\right) - k_{\phi_5}^{decay}\phi_5 + k_{\phi_6}^{deg}\phi_1\phi_6 \quad (26)$$

$$\frac{\partial \phi_6}{\partial t} = -k_{\phi_6}^{deg}\phi_1\phi_6 \quad (27)$$

where $k_{\phi_1}^{decay}$ and $k_{\phi_5}^{decay}$ are decay coefficients of MMP-2 ($0.0017\ s^{-1}$), and ligands ($0.0001\ s^{-1}$), respectively. $k_{\phi_5}^{deg}$ is a degradation coefficient of ECM ($1.04\times10^{6}\ M^{-1}s^{-1}$). $k_{\phi_1:\phi_2}^{on}$ is a kinetic association rate constant for binding TIMP-2 with MMP2 ($5\times10^{5}\ M^{-1}s^{-1}$) and its term physically represents the reduction of MMP-2 by the endogenous soluble inhibitor TIMP-2. $k_{\phi_3:\phi_4}^{on}$ is a kinetic association rate constant for binding the ternary complex with MT1-MMP ($1.95\times10^{4}M^{-1}s^{-1}$), which results in the release of activated MMP-2. $k_{\phi_2:\phi_3}^{on}$ is a kinetic association rate constant for binding TIMP-2 with MT1-MMP ($2.74\times10^{6}M^{-1}s^{-1}$), and $k_{\phi_4}^{off}$ is a kinetic dissociation rate constant of the ternary complex for unbinding TIMP2 and MT1-MMP ($2\times10^{-4}s^{-1}$). D_{ϕ_1}, D_{ϕ_3} and D_{ϕ_6} are the diffusion coefficients of MMP-2 ($68.8\times10^{-12}\ m^2/s$), TIMP-2 ($1.29\times10^{-12}\ m^2s^{-1}$) and ligands ($1.0\times10^{-15}\ m^2s^{-1}$), respectively. In particular, $\alpha_{\phi_2}\left(x_{base}^{f}\right)$ and $\alpha_{\phi_3}\left(x_{base}^{f}\right)$ represent secretion rates of TIMP2 ($1.0\times10^{-3}M\ s^{-1}$) and MT1-MMP ($1.0\times10^{-1}M\ s^{-1}$) at the root of a filopodium, respectively. x_{base}^{f} indicate the bases of filopodia, and MT1-MMP and TIMP-2 secretions at the membrane near the bases of filopodia are modelled as source terms [13].

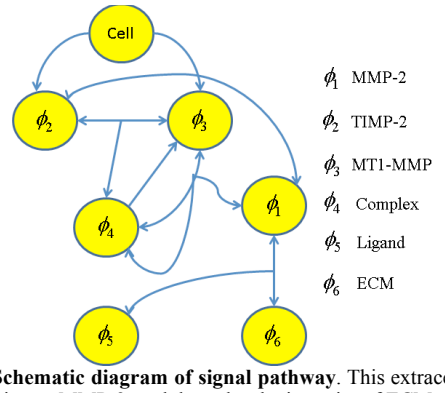

Figure 3: Schematic diagram of signal pathway. This extracellular signal pathway activates MMP-2, and degrades the integrity of ECM.

III. Results and Discussion

To simulate cancer cell migration in 3D ECM, two cases of simulations were performed to investigate dynamic behaviors of cancer cell migration in both soft and stiff ECMs. Accordingly, cancer cell models were initially embedded into two cases of ECM fiber network models; pore size is 1.0 μm and single fiber diameter of 32 nm for the stiff ECM, and pore size is 1.5 μm and single fiber diameter of 41 nm for the soft ECM. Previously, we modeled cell invasion into ECM fiber network, that is, cell extravasation into the ECM [8], and performed cell migration experiments using endothelial cells transfected with cytosolic GFP in the microfluidic device for the validation for the model [8]. We found that speeds of both tip and root of filopodia increase as the pore size is increased in experiments. The simulated speeds of both tip and root of filopodia, too, showed a good correlation to the experiments [8]. Here we assumed that cancer cell migration was started from its embedded condition in the ECM by the projection of some related ECM nodes located in the cell model towards the cellular membrane.

A selected simulated result shows that cellular morphology of each cell in both cases was elongated towards the direction of cell migration at t + 2400 seconds (**Figure 4A & 4B**). Interestingly, ECM densification was significantly observed in the trailing side of cell migration, and it was thicker in the stiff ECM than the soft ECM. Additionally, their orientations in densified regions were changed to align towards the direction of cell migration despite initial orientations of ECM fibers were isotropic. It appeared that cancer cell model in the soft ECM further migrated than that in the stiff ECM since the filopodia penetration dynamics

were experimentally observed to be the faster as filopodia interacts with the larger pore-sized ECM [8]. Furthermore, it is interesting to observe the size of ECM tunnel (or lumen) generated by cancer cell model. It has been known that as the speed of tip cell in the angiogenesis is the faster, the lumen is more narrowed [14]. Similarly, our simulations reveal a wide

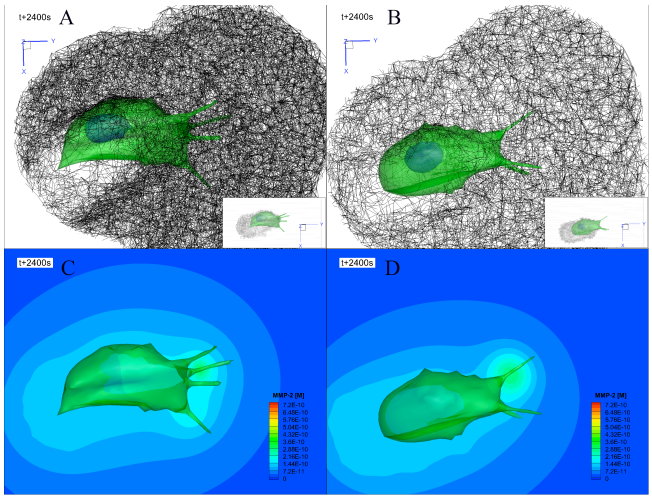

Figure 4: Simulation of cancer cell invasion into a densified ECM fiber network. Simulated cancer cell migration in two different ECM fiber network models with pore sizes of A) 1.0, and B) 1.5 μm at t + 2400 s. Green color indicate cellular and filopodial membranes, and blue color indicate a nuclear membrane. Black lines are ECM fibers with a diameter of 42 nm and a modulus of 1 MPa. Note that two different single fiber diameters of 34, and 41 nm are used for two ECM model with pore sizes of 1.0, and 1.5, respectively. Each inset in A) and B) indicates ECM tunnels (or lumens) generated during cancer cell migration. Selected simulation results of MMP-2 concentration distributions using simplified reaction-diffusion mass transfer model for MMP-2 activation in two different ECM fiber network models with pore sizes of C) 1.0, and D) 1.5 μm at t + 2400 s.

tunnel ECM tunnel and slightly slow cell migration in the stiff ECM model.

As simulated results shown in **Figure 4C& 4D**, as the cell made a deep invasion into the ECM domain, MMP-2 is secreted at the root of filopodia. Highest concentration of MMP-2 is found at the root of filopodia, and its concentration decays at the concentric circles from the root of filopodia. It should be noted that rates of secreted MMP-2 are varied depending on binding MT1-MMP with the ternary complex. In addition, all diffusion coefficients and some secretion rates of biochemical concentrations in the current model were assumed to be identical for two ECM fiber models. However, in fact, heterogeneous diffusion coefficients and secretion rates of biochemical concentrations should be considered in the future cell migration model since recent experimental observations have indicated that diffusion coefficient of bovine serum albumin (BSA) is decreased as the ECM is stiffer and a pore sizes of ECM network is reduced more [15].

IV. Conclusion

In conclusion, we successfully established a dynamic model for simulating cancer cell migration in 3D ECM to observe ECM remodeling due to mechanical interaction with cancer cell and its filopodia. The integrated cell model was incorporated from four individual dynamic models of filopodia penetration dynamics, intracellular dynamics, ECM fiber dynamics, and reaction diffusion mass transfer model. Our simulations reveal three interesting results in the stiff ECM comparing with the soft ECM: 1) slow speed of cancer cell migration, 2) thick ECM densification, and 3) the formation of wide ECM tunnel.

Future direction for the development of model will include the addition of intracellular signal pathway to guide the directed cancer cell migration cell towards the stiffer ECM, and be used to predict cancer metastasis including a collective migration mediated by both cell-cell and cell-ECM adhesions, epithelial-mesenchymal transition (EMT) -mediated mesenchymal cell migration, amoeboid migration in ECM.

Acknowledgment

This material is based upon work supported by the National Science Foundation (NSF), Science and Technology Center (STC) on Emergent Behaviors in Integrated Cellular Systems (EBICS) under Grant CBET-0939511. This research was also supported by the National Research Foundation Singapore through the Singapore MIT Alliance for Research and Technology's BioSyM IRG research program

References

[1] P. Lu, *et al.*, "Extracellular matrix degradation and remodeling in development and disease," *Cold Spring Harb Perspect Biol*, vol 3, no 12, pp. a005058, Dec. 2011.

[2] P. Lu P, V. M. Weaver, and Z. Werb, "The extracellular matrix: a dynamic niche in cancer progression," *J Cell Biol*, vol. 196, no. 4, pp. 395-406, Feb. 2012.

[3] P. Rørth, "Collective cell migration," Annu Rev Cell Dev Biol, pp. 123–135. *Annu Rev Cell Dev Biol*, vol. 25, pp. 407–429, Aug. 2009.

[4] A. G. Clark, and D. M. Vignjevic, "Modes of cancer cell invasion and the role of the microenvironment," *Current Opinion in Cell Biology*, vol. 36, pp. 13-22, Oct. 2015.

[5] P. K. Mattila, and P. Lappalainen, "Filopodia: molecular architecture and cellular function," *Nat Rev Mol Cell Biol*, vol. 9, pp. 446-454, June 2008.

[6] M.-C. Kim, *et al.*, "Integrating focal adhesion dynamics, cytoskeleton remodeling, and actin motor activity for predicting cell migration on 3D curved surfaces of the extracellular matrix," *Integrative Biology*, vol. 4, no. 11, pp. 1386–1397, Nov. 2012.

[7] M.-C. Kim, D. M. Neal, R. D. Kamm, and H. H. Asada, "Dynamic Modeling of Cell Migration and Spreading Behaviors on Fibronectin Coated Planar Substrates and Micropatterned Geometries," *PLoS Comput Biol*, vol. 9, no. 2, pp. e1002926, Feb. 2013.

[8] M.-C. Kim, *et al.*, "Cell Invasion Dynamics into a Three Dimensional Extracellular Matrix Fibre Network," *PLoS Comput Biol*, vol. 11, no. 10, pp. e1004535, Oct. 2015.

[9] C. J. Kim, "A coordinate-free form of the finite gradient in discretizing scalar and momentum diffusion," *In proceedings of the 4th JSME-KSME Thermal Engineering Conference*, Kobe, Japan, 2000.

[10] G. I. Bell GI, "Models of specific adhesion of cells to cells," Science, vol. 200, pp 618–627, 1978.

[11] L. Yang, *et al.*, "Mechanical properties of native and cross-linked type i collagen fibrils," *Biophys J*, vol. 94, no. 6, pp. 2204-2211, Mar.2008.

[12] N. E. Deakin, and M. A. J. Chaplain, "Mathematical modeling of cancer invasion: the role of membrane-bound matrix metalloproteinases," *Frontiers in Oncology*, vol. 3, pp. 1–9, Apr. 2013.

[13] R. Poincloux, F. Lizárraga, and P. Chavrier, "Matrix invasion by tumour cells: a focus on MT1-MMP trafficking to invadopodia," *J Cell Sci*, vol. 122, pp. 3015-3024, 2009.

[14] L. Wood, R. Ge, R. Kamm, and H. Asada, "Nascent vessel elongation rate is inversely related to diameter in in vitro angiogenesis," *Integrative Biology*, vol. 4, no. 9, pp.1081-1089, July 2012.

[15] P. Chaudhuri, et al., "Extracellular matrix stiffness and composition jointly regulate the induction of malignant phenotypes in mammary epithelium," *Nature Materials*, vol. 13, pp. 970-978, June 2014.